

Final Report for OTKA K72664

November 7, 2013

Substantial progress was made regarding each of the four research aims as described below. Research projects involving experiments proceeded somewhat slower than planned, therefore we are still actively working on manuscripts that will publish results generated during this proposal. These results are explained in greater detail below.

The major change in the investment budget was forced by the governmental purchasing ban on computational equipment.

1 Progress on aim 1 “To study collective cell migration, in vitro.”

Collective cell motility is an important aspect of several developmental and pathophysiological processes. Despite its importance, the mechanisms that allow cells to be both motile and adhere to one another are poorly understood.

1.1 Statistical measures of collective 2D cellflow

In [1] we demonstrated that endothelial cells exhibit a capacity for coordinated (collective) migration in culture. In the absence of directed expansion of the whole monolayer, these cells exhibit a globally undirected, but locally correlated streaming behavior.

We suggested that the average flow field around moving cells can serve as a measure sensitive to the local cell movement pattern. For a given configuration of cell positions and velocities this procedure assigns reference systems co-aligned with the movement of each cell, and averages the velocity vectors observed at similar locations (e.g., immediately in front, behind, left and right).

Such statistical characterization of the spontaneous streaming motion revealed that cells move in locally anisotropic, 50-100 μm wide and 200-300 μm long streams, which form and disappear at random positions. Remarkably, very similar correlation structures are seen in all three types of endothelial cell monolayer cultures investigated, irrespective of the underlying extracellular matrix substratum used. In subconfluent cultures, where fewer constraints are imposed by the behavior of adjacent cells, the correlated (co-moving) area shrinks.

Another, longer-term property of collective flow is its ability to maintain adjacency of cells. The amount of mixing within the monolayer is indicated by how quickly initially adjacent cells separate from each other. Thus, we calculated the time-dependent average distance between cell pairs that are adjacent in a given reference frame. These studies revealed that despite the presence of streams, cell mixing is substantial in the monolayers: with a good approximation, movement of adjacent cells can be considered as independent persistent random walks.

1.2 Intercellular adhesions regulate collective flow

While cell-cell adhesion is expected to strongly influence collective flow within a cellular monolayer, its actual role is little understood. Most models that are widely used in multicellular simulations are not sensitive to the relative motion of adjacent cells; for example in the cellular Potts model (CPM), the “energy” or goal function depends only on the instantaneous configuration and lack temporal persistence or memory. Yet, previous experimental reports indicated altered collective flow when cell-cell adhesion was perturbed. In [2] we explored the spontaneous streaming movements in epithelial monolayer cultures, and demonstrated that when normal cell-cell adhesion is perturbed by calcium chelation, the correlated streams become narrower and the shear between cells is increased. Our results clearly show that cell adhesion molecules can play a role in shaping the spontaneously emerging streams in confluent cultures. In particular, correlations perpendicular to cell movement are significantly decreased as cell adhesion is weakened. Weaker cell adhesion allows the cells to change neighbors more easily, and thus have a larger velocity difference (intercellular shear) between adjacent cells.

1.3 Interplay between cell polarity, motion persistence and collective cell stream organization

In a manuscript close to completion [3] we analyzed how experimental tuning of cell polarity persistence, a key parameter in our suggested model [1], alters the collective flow within the monolayer. Persistent spontaneous cell motility is thought to reflect intracellular polarity, a biochemical state created by an instability of positive feedback regulation. While the molecular mechanism responsible for front/rear polarity is poorly explored in endothelial cells, in other cell types it involves localized accumulation of phosphatidyl-inositols (PIs), in particular the phosphorylated PIP_2 and PIP_3 forms, as well as the spatially restricted activity of small GTPases, such as Rac1. Motivated by these findings, we used pharmacological inhibitors of PI3K kinase, a key enzyme in PI interconversion, as well as an inhibitor of Rac1. Cell persistence data were estimated from time-lapse recordings by numerically integrating Particle Image Velocimetry (PIV)-obtained velocity fields. These experiments proved that we can control cell motion persistence within the monolayer in a dose-dependent manner.

To characterize how cell movements are correlated within the monolayer, we calculated $\vec{V}(\vec{x})$, the average flow field in a reference frame co-aligned with a typical moving object [1]. As Fig. 1a demonstrates, the PIV data yield very similar flow fields as those reported previously for HUVEC cells: cell motion is similar in front of and behind the cells, while this similarity disappears quickly in the direction perpendicular to the motion. When cell polarity is perturbed, this local anisotropy is reduced (Fig. 1b).

Various $\vec{V}(\vec{x})$ flow fields can be conveniently compared along lines parallel or perpendicular to the direction of the local motion (Fig. 1c,d). To obtain characteristic lengths of the streams, $V_x(x, 0)$ and $V_x(0, y)$ were fitted by exponential functions $\exp(-|x|/\xi_{\parallel})$ and $\exp(-|y|/\xi_{\perp})$, respectively. The obtained correlation lengths ξ_{\parallel} and ξ_{\perp} change, in a dose dependent manner, when the function of PI3K was perturbed. In fact, we found a close relationship between the persistence length of cell trajectories and the ξ_{\parallel} , ξ_{\perp} correlation lengths of the velocity fields, irrespective of the perturbing reagent used (Fig. 1e).

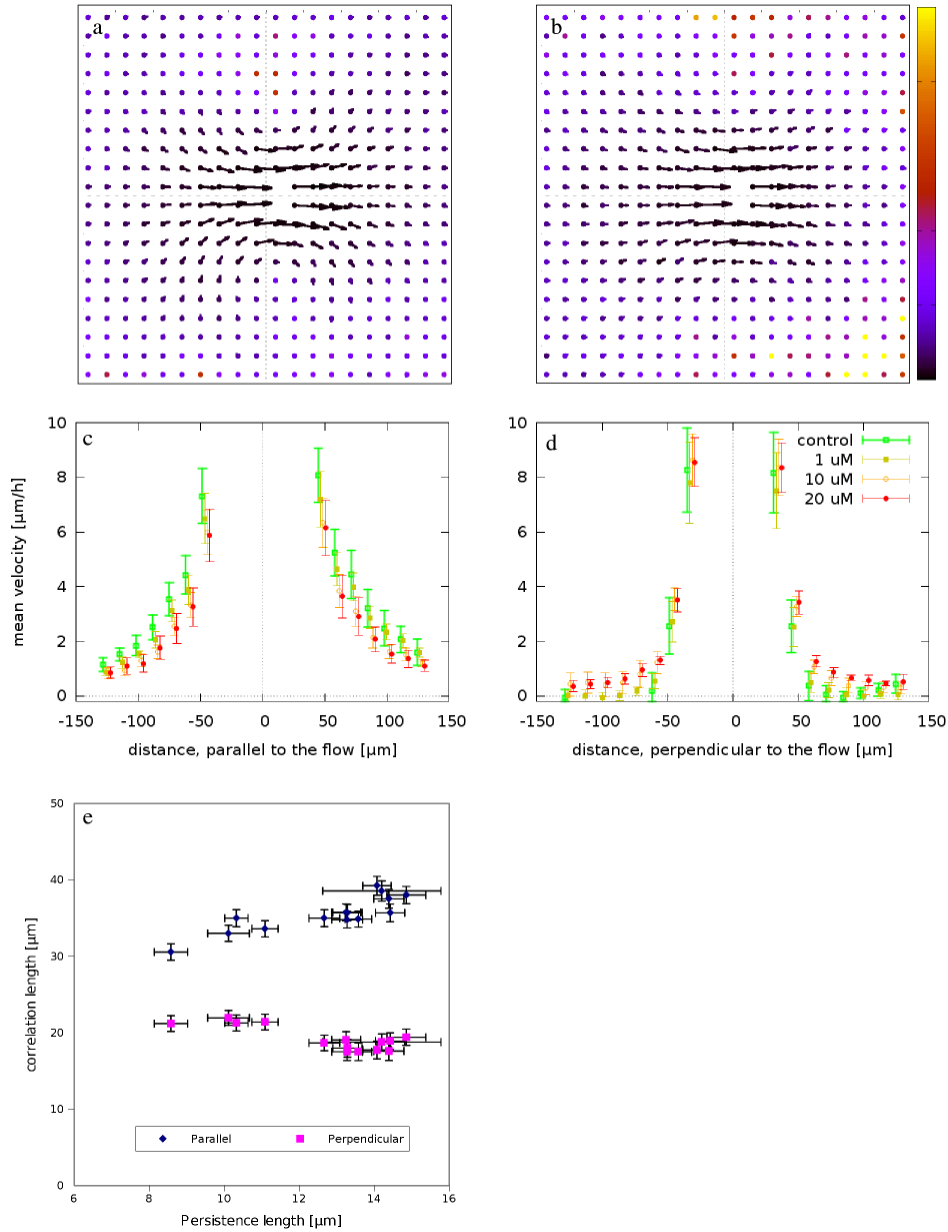


Figure 1: Motion persistence determines spatial correlations of the monolayer flow. The average flow field \vec{V} was calculated around moving cells in control (a) and drug-treated cultures as described in [1]. As an example, \vec{V} obtained in the presence of 20 μM LY294002, a pharmacological inhibitor of PI3K is shown in (b). Velocities are represented as displacement vectors, extrapolated for a one hour interval. The color code indicates data reliability, as normalized SEM (SEM/mean) values. Grid spacing is 25 μm . To compare monolayer flows, we plotted the average \vec{V} values along (c) and perpendicular (d) to the direction of local motion. Fitting these curves with an exponential cutoff yields our correlation lengths, one along and one perpendicular to the local flow. e: Correlation lengths vs the persistence length of the motion fall onto a universal curve irrespective of the method used to perturb cell polarity.

2 Progress on aim 2 “To study the reciprocal coupling between cell motility and ECM assembly”

The importance of extracellular matrix (ECM) during morphogenesis and organogenesis is comparable to that of the cells. In addition to providing structure to the interstitial spaces between cells, the ECM acts as a scaffold for cell adhesion. Cellular adhesion results in a physical coupling of the intracellular cytoskeleton and the extracellular environment, the ECM. This contact mediates cell migration (movement relative to the ECM) and also allows the cells to exert mechanical forces.

2.1 Cell invasion into an ECM environment

Cell invasion from an aggregate into a surrounding extracellular matrix is an important process during development and disease, e.g., vascular network assembly or tumor progression. In [4] we considered a simple, but frequently utilized in vitro experimental setting which consists of a cell aggregate placed within a three dimensional ECM (usually collagen I) gel. As we focused on the role of cell motility during the invasion process, we performed the invasion experiments in the presence of a cell division inhibitor Q50. We demonstrated that after one day in culture the proliferation-inhibited cells form very similar structures to those observable in 3D cultures of normally dividing cells. Of particular interest are the radially oriented, elongated cells that invade the gel. Some of these cells form multicellular chains.

To describe the behavior emerging from autonomous cell motility, cell-cell adhesion and contact guidance by extracellular matrix filaments, we proposed a suitably modified cellular Potts model. We considered an active cell motility process in which internal polarity is governed by a positive feedback from cell displacements. We demonstrated that such a mechanism can result in highly persistent motion when constrained by an oriented extracellular matrix structure. The model allowed to explore the interplay between haptotaxis, matrix degradation and active cell movement. We showed that for certain conditions the cells are able to both invade the ECM and follow ECM tracks. Furthermore, we argued that enforcing mechanical equilibrium within a bulk cell mass is of key importance in multicellular simulations.

Our proposed model suggests that the increased persistence during the cell invasion process may be a consequence of two effects: (i) a space-constrained polarized motion and (ii) adhesion to and degradation of the ECM. The former is more relevant when cells move in established microchannels, while the latter is relevant for “tip” cells at the front of invading sprouts. If cells are able to degrade the ECM, then the tendency to invade is determined by the two time scales characterizing intracellular polarity and ECM degradation. Even if ECM degradation is slow, the model allows invasion of cells that maintain intracellular polarity for a sufficiently long time. According to our simulations, haptotaxis and ECM degradation (without active cell motility coupled to an autonomous, internal polarity) destabilizes multicellular sprouts as each cell tries to invade the ECM. In contrast, when both haptotaxis and polarized motion is present in the model, even a homogenous cell population organizes into multicellular sprouts within an inhomogenous ECM environment.

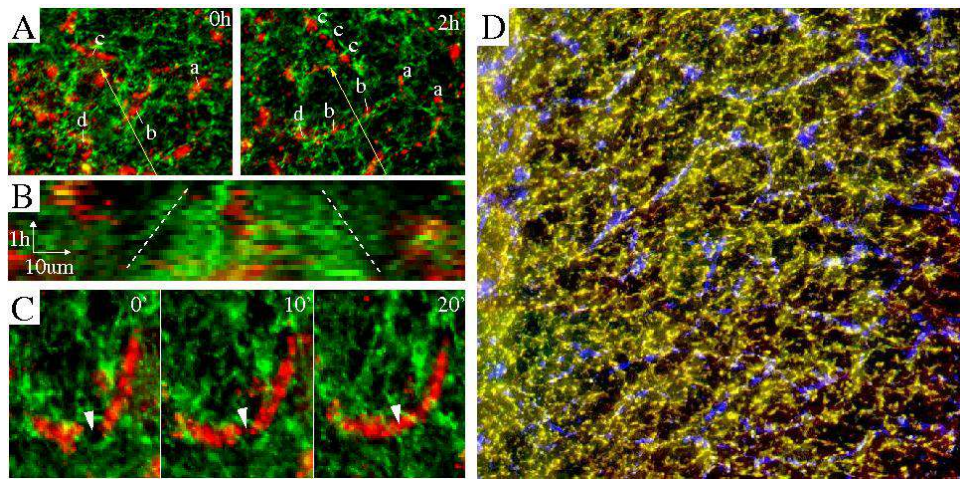


Figure 2: Fibronectin dynamics during vascular assembly. A: Two time lapse frames showing the initial and end stage of a vascular link formation. Red: endothelial cells marked by a cell surface epitope, QH1. Green: Fibronectin, visualized by microinjected immunofluorescence. Labels a-d mark cells migrated from the same cluster. B: Spatiotemporal plot (“kymograph”) of epifluorescence intensity perpendicular to the sprout (along the line marked by the yellow arrow in panel A). The gradual ECM enrichment along the vascular vessel is evident. C: vascular cells can join and form a segment without following fibronectin filaments. D: Pulse (red) - chase (green) Fibronectin immunolabeling, separated by 4 hours. The yellow colors indicate that antibodies from both the first and second round of labeling found the same targets – that is, no new Fibronectin filaments were generated during the elapsed time. Blue: QH1 immunofluorescence label of endothelial cells.

2.2 Fibronectin dynamics during vascular network formation

In fixed embryos, as well as in deconvolved time-lapse sequences, we analyzed the co-distribution patterns of an ubiquitous ECM component, fibronectin, and the endothelial/angioblast markers QH1, TAL1, and TIE1 [5]. Systematic statistical analysis of the data shows that fibronectin does not pre-pattern the future vascular polygons, and the motion of QH1 positive cells is independent of the direction of adjacent fibronectin fibers. Fibronectin, however, accumulates very early on endothelial basal surfaces, sometimes an enrichment can be detected before the expression of the QH1 marker. Time-lapse data, surprisingly, show that the fibronectin is recruited and remodeled from the ECM meshwork surrounding the mesoderm (Fig. 2). To perturb fibronectin assembly, we introduced the assembly-blocking 70 kDa fibronectin fragment, both in vivo and in cultures where endothelial cells sprout in collagen gels. We found that (i) in vitro blocking fibronectin assembly after the completion of the first linear structures does not have an adverse effect, while (ii) it can interfere with the process if fibronectin assembly is blocked when only scattered endothelial cells are present in the gel. We failed to observe any adverse effect in vivo with the microinjected 70 kDa fibronectin fragment. By labeling fibronectin filaments in the yolk, we showed that some of the embryonic fibronectin used during blood vessel assembly is taken up from the yolk, with the implication that the embryo is supplied with a large pool of pre-made fibronectin filaments. Based on the data currently available, we hypothesize that the role of fibronectin is stabilizing an already established vascular segment [6].

3 Progress on aim 3 “Three-dimensional mapping of embryonic tissue flows. Estimating the intrinsic mechanical stress and material properties of the tissue”

3.1 ECM fluctuations

Extracellular matrix (ECM) movements and rearrangements were studied in avian embryos during early stages of development in a collaboration with Drs Rongish and Little at the University of Kansas Medical Center [7]. We demonstrated that the ECM moves as a composite material, whereby distinct molecular components as well as spatially separated layers exhibit similar displacements. Using scanning wide field and confocal microscopy we showed that the ECM velocity field is smooth in space and thus ECM movements are correlated even at locations separated by several hundred micrometers. Velocity vectors, however, strongly fluctuate in time. The autocorrelation time of the velocity fluctuations is less than a minute. We argue that the likely source of the fluctuations is individual cell contractile activity. Numerical suppression of the fluctuations yields a persistent movement pattern that is shared among embryos at equivalent stages of development. The high resolution of the velocity fields allows a detailed spatio-temporal characterization of important morphogenetic processes, especially tissue dynamics surrounding the embryonic organizer (Hensen’s node).

ECM filaments are especially suitable to map tissue movements since the ECM meshwork (unlike a cell layer) is an inert object incapable of active movements. In addition, the ECM is the microenvironment for some embryonic cell types like mesenchymal cells or early vascular precursor cells. Thus, movement of the whole ECM meshwork is expected to carry any passive,

adhesive cell. Furthermore, considering the tissue as a composite material of cells and ECM, we expect that even passive objects not adherent to the ECM would move in a similar fashion. In fact, the co-movement of ECM and injected microbeads was observed in recent experiments exploring heart development [8]. These studies also demonstrated the co-movement of endogenous and microinjected exogenous ECM components.

3.2 Tissue movements during early heart development

By analyzing the movements of immunolabeled ECM components (fibronectin, fibrillin-2) and TIE1 positive endocardial progenitors in time-lapse recordings of quail embryonic development, we demonstrated that the transformation of the primary heart field within the anterior lateral plate mesoderm (LPM) into a tubular heart involves a precise co-movement of primordial endocardial cells with the surrounding ECM [8]. Thus, the ECM of the tubular heart contains filaments that were associated with the anterior LPM at earlier developmental stages. Moreover, endocardial cells exhibit surprisingly little directed active motility, that is, sustained directed movements relative to the surrounding ECM microenvironment. These findings point to the importance of large-scale tissue movements that convect cells to the appropriate positions during cardiac organogenesis.

This work represented the first demonstration of ECM filaments being translocated and incorporated into a future organ. The maintenance of anterior-posterior positional order during the time the cardiac jelly is accumulated has implications for the establishment/maintenance of ECM-bound morphogen gradients. If gradients of morphogens are pre-established outside of the forming heart tube, and if the ECM-bound morphogens are then swept into the heart with the same relative positions, a corresponding anterior-posterior morphogen gradient may be maintained. Similarly, any left/right asymmetry in the distribution of ECM molecules/bound morphogens in the lateral plate would likely be maintained in the heart tube.

The most likely interpretation for the shared large-scale movement pattern between the two ECM components and endocardial progenitors is a model whereby the whole tissue (cells and the associated ECM as a composite material) moves and deforms in response to mechanical forces, exerted by cells within the heart field or in adjacent tissue layers. The finding that microinjected inert objects also translocate to the forming heart, in an identical manner, is entirely consistent with such a view. As we have shown in this work, active motility of endocardial progenitors, defined as the difference between the local cell and ECM displacements, is much smaller and more random than the movements characterizing tissue deformation.

3.3 Characterizing tissue stresses during early heart development

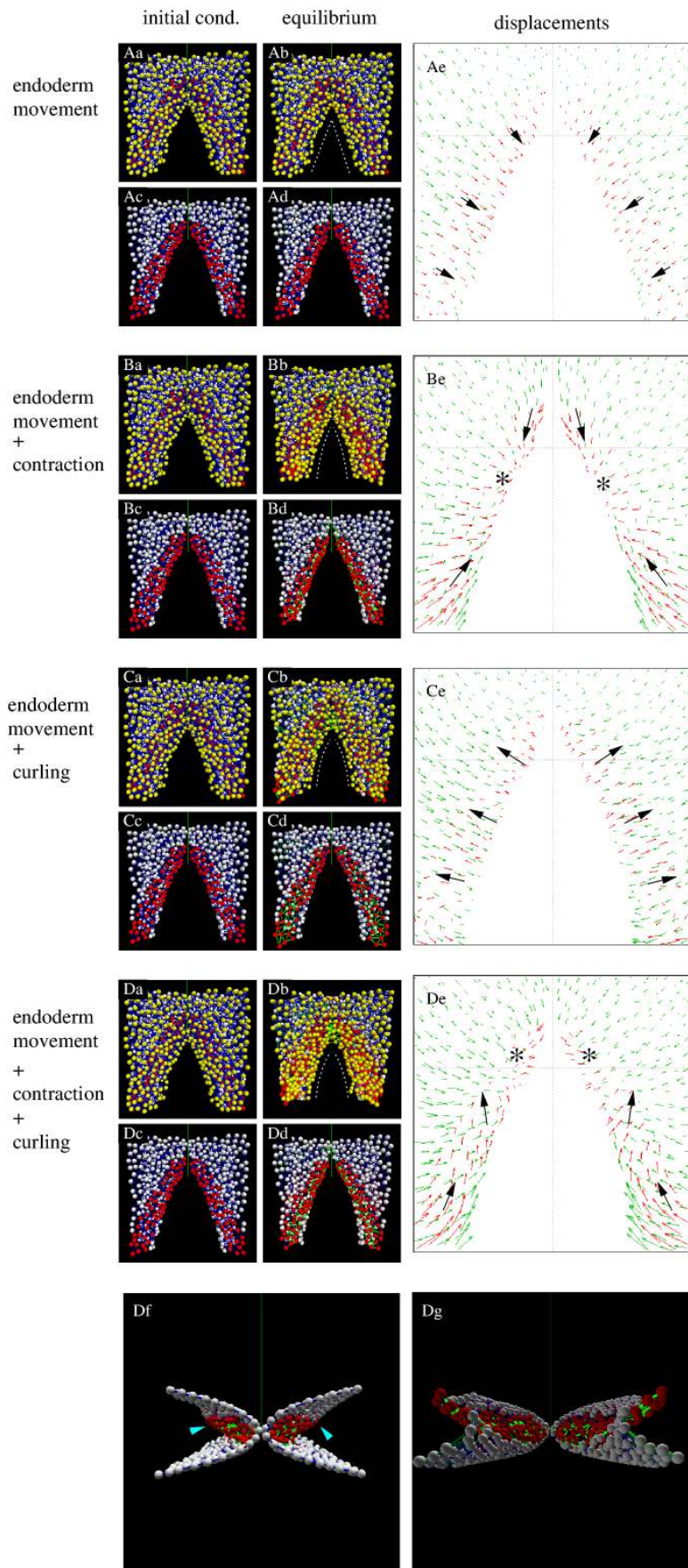
Using mechanical perturbations to remove the constraining influences of surrounding tissues, we demonstrate in [9] that myocardial progenitor fields undergo a series of coordinated deformations that are able to propel their displacements. To alter the tissue mechanics of early heart formation, we used tungsten needles to perform a series of incisions through the endoderm and underlying splanchnic mesoderm in selected regions within the anterior embryo (Fig.3). Perturbations to the ventral midline endoderm induce separation of cardiac progenitor fields, i.e. the formation of two heart-like structures.

Incisions targeted laterally, at approximately 100 μm distance from the lateral edge of the heart field (Fig.3C), as well as those placed medially to the myocardial fields, through the paraxial meso-

derm or notochord, had very little or no effect on the morphogenesis of either the heart field. In contrast, 500-600 μm long incisions within the myocardial field, parallel to the anterior-posterior axis, result in striking deformations (Fig. 3D, Da). Immediately after the incision, the unconstrained wound edges of the myocardium bend ventrally and medially. Later, a portion of the heart field that initially was located posterior to the incision advanced in the anterior direction, past the wound edge. The morphology as well as the processes within the perturbed myocardium are demonstrated in a schematic form in Fig. 3Db.

Even more pronounced myocardial changes were achieved when 200-300 μm -long incisions

Figure 3 (*preceding page*): Typical phenotypes, induced by localized incisions through the endoderm and splanchnic mesoderm. A: location of incisions (labeled B-E) that result in phenotypes shown in panels B-E. Myocardial fields are schematically represented in red. B,C,D,E: Time-lapse image sequences of perturbed myocardial development. Red: antibody-labeled fibronectin ECM, green: myocardial cells. Contour lines delineate the wound edges at the onset of recording, that is, 0.5-1.5 h post-incision. Time elapsed during recording is indicated on image panels. Scale bars: 100 μm unless otherwise indicated. Bd, Ca, Da: Myocardium visualized at the conclusion of the recordings by post-fixation MF20 antibody (green) and confocal imaging. B: An incision through the endoderm at the ventral midline leads to the failure of midline fusion and the formation of two lateral hearts, a phenotype referred to as *cardia bifida*. Ba-Bc images of the left myocardial field of a CMLC2::GFP-transfected embryo. Color-code indicates dorso-ventral position of the labeled cells. Contour lines illustrate the position of the foregut. The same cell groups are marked by an arrow and an arrowhead. Myocardial cells become increasingly ventral, as indicated by the change in color from blue/green to yellow/red at the lateral edge of the myocardial field. C: An incision through the endoderm and the underlying splanchnic mesoderm lateral to the myocardial fields has only minor effects on heart development and is compatible with myocardial fusion at the midline. D: Bilateral, longitudinal incisions through the myocardial fields and the endoderm. The region marked by the white rectangle on the left panel is shown in detail in the adjacent panels. Db: a schematic representation in a ventral view of the mechanics within the perturbed myocardial field. The differentiating myocardium (dark green), attached to the surrounding mesoderm (light green), is undergoing a contraction along the medial edge (magenta arrows). At the same time, the myocardium is bending dorsally to generate a cup-shaped groove (illustrated by cyan arrows). The incision (red contour line) introduces an unconstrained edge, which bends medially (cyan arrows). The forces generated in the myocardial field posterior to the incision propels the latter anteriorly (blue segmented arrow) past the wound edge. E: Bilateral, medio-lateral incisions, perpendicular to the foregut, through the endoderm and the underlying myocardium and splanchnic mesoderm. Ea: cellular resolution image sequence depicting myocardial cells curling ventrally at the wound edge, within the area marked by a white rectangle in panel E. The color code represents dorsal-ventral position. Eb: a schematic representation of the mechanics within the perturbed myocardial field, with the same notations as used in panel Db. The incision (red contour line) separates the myocardium and the adjacent non-myocardial mesoderm from the anterior tissues. As in Db, the force generated by the uniform contraction (dorsal bending) of the myocardial field posterior to the incision propels the latter anteriorly (blue segmented arrow) past the wound edge. This process continues as bending is initiated at progressively more posterior levels of the differentiating myocardium and thus propels the formation of a characteristic spherical curl at the wound edge. Ec and Ed are images of transverse sections taken post-fixation at the lines indicated in panel E. Note that the myocardium forms pronounced spherical cusps posterior to the incision site (Ec), whereas the endoderm remains relatively planar. At the incision site (Ed), deformed (curled) myocardium is found ventral to the endoderm. En – endoderm, mc – myocardium, nc – notochord, nt – neural tube, s – somite; D – dorsal, V – ventral, L – left, R – right. Scale bars in Ec and Ed: 50 μm .



were placed perpendicular to the AP axis, within the region marked with a white bracket in Fig. 3A. As seen in Fig. 3E, myocardial sheets continue to move anteriorly, and the wound edge advances past the incision site and bends over the ventral surface of the endoderm. This rolling forward movement of the myocardial fields drives cells at the wound edge to progressively more ventral and posterior positions (Fig. 3Ea). Figures 3Ec and Ed illustrate the cross-sectional anatomy of the perturbed embryo shown in Fig. 3E. The two sections were obtained caudal to the posterior wound edge and at the level of the incision site, respectively. These sections illustrate the cup shaped myocardial structures that form by progressive ventral curling that eventually result in their contact with the ventral side of the endoderm.

To interpret the results of microincision experiments, we first note that the endoderm adjacent to the wound does not exhibit substantial morphological changes. Thus, the observed myocardial structures are likely to develop autonomously, without mechanical driving from the adjacent endoderm. We propose that the observed deformations are a cumulative result of forces acting within, and specific to the myocardial sheet. As illustrated in schematic forms in Figs. 3Db and Eb, the differentiating myocardium is attached to the surrounding non-myocardial mesoderm. We propose that the myocardium contracts along the medial edge (as illustrated by magenta arrows in Fig. 3Db and Eb). At the same time, the myocardium also develops forces that curl the sheet to produce a convex dorsal surface in a spatially uniform manner – thus, the same curvature is expected in all directions within an unconstrained myocardial piece of epithelium. Mechanical constraints at the myocardial-mesodermal tissue boundaries restrict most of this curling along the head-tail (A-P) axis, but permit bending dorsally in the lateral direction to generate a groove (panels 3D-Db and E-Ed). We hypothesize that the curling and the contraction of the medial myocardial edge drive the anterior-directed movements of the myocardium relative to the endoderm. The incisions (red contour lines in Figs 3Db and Eb) introduce unconstrained (unattached) edges, which can bend further in the absence of mechanical constraints (cyan arrows). The A-P component of the curling activity, posterior to the incision, propels the myocardium anteriorly, past the wound edge (cyan segmented arrows in Figs 3Db and Eb). During normal development the myocardial field is located in the close vicinity of the AIP. If the latter undergoes a uniform contraction, then the ECM-mediated mechanical coupling between the endoderm and myocardium/mesoderm leads to

Figure 4 (*preceding page*): Tissue movements resulted by various active cell behaviors. A: A prescribed medio-caudal movement of the endoderm rolls the myocardium medially, contributing to the inversion of the myocardial field. B: Contraction of the medial aspect of the myocardium narrows the foregut and reduces its curvature. C: Uniform curling of the myocardium moves the myocardial field laterally and anteriorly, as well as widens the foregut. D: The combination of the three effects moves most of the myocardial field antero-medially relative to the surrounding tissue movements. Panels a and b show all particles, while the endoderm and associated cell-cell connections are removed from panels c, d. The initial configuration is shown in panels a, c. The mechanical equilibrium resulted by the prescribed cellular activity is shown in panels b, d. The shape of the foregut portal is indicated by white dotted lines in panels b. Panels e show the tissue displacements during the simulations. Red and green arrows indicate movements of the myocardium and both surfaces of the folded mesoderm, respectively. Black arrows are guides for the eye, indicating the local direction of myocardial movements. Asterisks mark contraction centers. Panels Df and Dg show, from anterior and posterior aspects, the combined effects of all three cellular activities. Arrowheads indicate a developing bulge of the myocardium into the coelomic space.

the overall postero-medially directed motion of the mesoderm and myocardium.

To show the biomechanical feasibility of our suggested mechanism of myocardial morphogenesis, we developed a cell-resolved mechanical model of the myocardium, and adjacent tissues: the mesoderm and endoderm. In our model, cells and their mechanical connections with adjacent cells are represented by particles and interconnecting elastic beams. The beams can be compressed and stretched, bent and twisted. The advantage of explicit cell-cell contact representation is that we can prescribe certain activities to a subpopulation of cells.

We envision tissue dynamics as a set of processes in which cell activities, like cell shape changes or alterations in mechanical contacts between cells, are accommodated by an elastic deformation of the surrounding tissue. We argue that the tissue is always in mechanical equilibrium, that is, changes in cell activity such as contraction are slow compared to the time needed for the environment to accommodate these changes. Thus, we explore by computational simulations, how certain cellular activities change the tissue configuration in which mechanical equilibrium is satisfied.

We explicitly consider three distinct cellular activities. 1. The medial aspect of the myocardium contracts – simulated by a prescribed shortening of the interparticle bonds. 2. A uniform and isotropic curvature of the myocardial sheet is modeled by changing the equilibrium directions of the links that connect a myocardial particle to its neighbors. 3. The endoderm moves medio-caudally to regress the AIP. We do not aim to model the driving forces of this process, instead we prescribe a centripetally directed displacement field along the AIP and at the ventral endodermal surface – a displacement field commensurate with empirical observations. After prescribing a combination (or all) of these activities, by numerical simulations we determine the new configuration in which the surrounding tissue accommodates these cellular activities and the whole system reaches mechanical equilibrium. As Fig. 4 demonstrates, the combination of myocardial contraction and curling moves the myocardium antero-medially in agreement with empirical findings. The foci of myocardial contraction are also moved towards the midline. As a further realistic model outcome, the myocardium and the surrounding endoderm protrude as a groove into the coelom. Therefore, these simulations demonstrate that due to the mechanical constraints of the adjacent tissues, simple myocardial cellular activities can result in tissue deformations that are markedly distinct from the prescribed behavior, and show a great degree of similarity with the empirically observed movement patterns.

The model (with the same parameters) can also reproduce myocardial movements after mechanical perturbations. In simulations where the links crossing the embryonic midline at the anterior-most aspect of the AIP were removed, the simulated “wound” opens up, and the movement of the myocardium is consistent with two attractive foci, one at each side. Furthermore, a mediolateral incision in the myocardium and the surrounding mesoderm yields a ventrally curled myocardial structure. Thus our computational model demonstrates that our proposed autonomous myocardial activities, contraction and curling, are capable of explaining both normal and perturbed development.

4 Progress on aim 4 “To develop continuum and cell-resolved models of collective cell motility and embryonic or artificial tissue development.”

4.1 Computational model for collective cell streaming within a monolayer

To explain the reported empirical findings in [10], we expanded the widely used cellular Potts model (CPM) to include active cell motility. In particular, for spontaneous directed motility we assumed a positive feedback between cell displacements and cell polarity. The resulting model was studied with computer simulations, and was shown to exhibit behavior compatible with experimental findings. In particular, in monolayer cultures both the speed and persistence of cell motion decreases, transient cell chains move together as groups, and velocity correlations extend over several cell diameters. As active cell motility is ubiquitous both in vitro and in vivo, our model is expected to be a generally applicable representation of cellular behavior.

We find it remarkable that a pair of parameters characterizing the persistence of cell polarity, T , and the bias this cell polarity has on stochastic cell movements, P , yield individual cell speeds, persistence times in the correct range as well as a collective behavior comparable with the empirically observed streams. In particular, $T = 5$ minutes is a plausible value for the time needed to alter cell polarity. With this value, it is possible to obtain cell speeds in the range of 20-40 $\mu\text{m}/\text{h}$ within monolayers and 50 $\mu\text{m}/\text{h}$ for individual cells. Our empirical data yielded cell speeds between 10 and 30 $\mu\text{m}/\text{h}$ for monolayers. A similarly close, and independent agreement is obtained for the persistence times, at approximately one hour both in the model and in the experiments. The spatial structure of streams is strongly anisotropic, being approximately 200-300 μm long and 100 μm wide in both the experiments and in the simulations.

4.2 Augmenting the self-propelled cellular potts model with explicit cell-cell contacts

In [2] we demonstrated that decreasing cell adhesion induces narrower and more anisotropic cell streams, reminiscent of decreasing the Taylor scale of turbulent liquids. To explain our empirical findings, we proposed a model that represents the dual nature of cell-cell adhesions. Spring-like connections provide mechanical stability, while a cellular Potts model formalism represents surface-tension driven attachment. The proposed model established a link between a viscosity-like feature of emergent multicellular motility and subcellular dynamics such as the lifetime of a cell adhesion structures.

A further, significant difference between the proposed CPM and most particle models with alignment interaction is that the latter is a polar interaction (when colliding, particles tend to move in a parallel direction) while the interaction between CPM cells is apolar: cells can readily glide in opposite directions, similar to the dynamics of self-propelled rods. The introduction of springs is designed to penalize relative movement between cells, acting as a kind of friction, therefore a polar interaction can be introduced gradually into the proposed model by tuning the parameters of connectivity dynamics. In particular, the appearance of a single vortex behavior seen for stable and sufficiently strong springs is a manifestation of a polar order, similarly to the development of a long range polar order by increasing the friction in the interacting rod model. Our and other related

modeling efforts thus suggest that epithelial monolayers are in a globally disordered, but locally nematic order state, which can transition into a globally ordered migratory state by slight adjustments of cell adhesiveness.

4.3 Role of cell-cell contacts to guide motility

Collective cell motility and its guidance via cell-cell contacts is instrumental in several morphogenetic and pathological processes such as vasculogenesis or tumor growth [11]. Multicellular sprout elongation, one of the simplest cases of collective motility, depends on a continuous supply of cells streaming along the sprout towards its tip. The phenomenon is often explained as leader cells pulling the rest of the sprout forward via cell-cell adhesion. Building on an empirically demonstrated analogy between surface tension and cell-cell adhesion, we demonstrated in [10] that such a mechanism is unable to recruit cells to the sprout. Moreover, the expansion of such hypothetical sprouts is limited by a form of the Plateau-Taylor instability. In contrast, actively moving cells – guided by cell-cell contacts – can readily populate and expand linear sprouts. We argued that preferential attraction to the surfaces of elongated cells can provide a generic mechanism, shared by several cell types, for multicellular sprout formation. The model investigated in [10] results in sprouts that are (i) able to recruit cells from the base, and (ii) are linear structures (iii) with a steady expansion speed. Furthermore, (iv) cells in the sprout can mix and change their order. To achieve this behavior we needed both persistently moving tip cells as well as preferential adhesion to elongated cells [12].

4.4 Cytoskeletal dynamics

Nucleokinesis, the movement and positioning of the cell nucleus, is an essential process within a diverse variety of organisms and cell types. Despite the developmental and functional importance of nuclear positioning in vertebrate cells, the underlying mechanics of force generation is not well explored. The complex nature of nuclear movement is indicated by the different, sometimes contradictory mechanisms proposed recently. In [13] we investigated the mechanical aspects of nucleokinesis using mouse radial glia-like and C6 rat glioma cell types in culture. The radial glia-like cell population has been in the focus of research interest as they may function as primary progenitors or neural stem cells. Surprisingly, instead of inhibiting nucleokinesis, inhibition of myosin II triggers an increased nuclear motility after a pronounced morphological transition in both cell types. When Myosin II is blocked, cells acquire a highly elongated bipolar shape, similar to the cell morphologies obtained on narrow adhesion stripes or to the morphology of the C6-R radial glia-like subclone of the C6 cell line. When myosin II is active, time-resolved traction force measurements indicate a pulling force between the leading edge and the nucleus of C6 cells. In the absence of myosin II activity, traction forces during nucleokinesis are diminished below the sensitivity threshold of our assay. By visualizing the centrosome position in C6 cells with GFP-centrin, we demonstrated that in the presence or absence of myosin II activity the nucleus tends to overtake or lag behind the centrosome, respectively. We interpreted these findings with the help of a simple viscoelastic model of the cytoskeleton consisting active contractile and passive compressed elements.

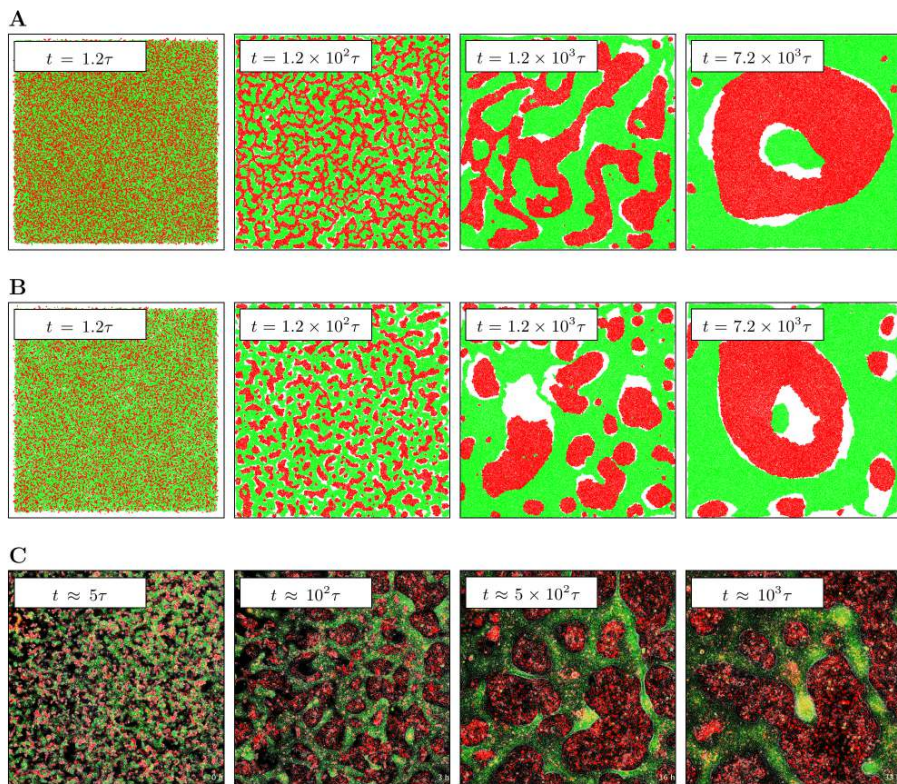


Figure 5: Morphologies characterizing the segregation of a SPP mixture at 50:50 (a) and 40:60 (b) coverage ratios. Red particles are more motile than green particles. White areas are devoid of particles – uniform clusters can achieve higher local cell density than areas where the two particle types are intermixed and their movement is less correlated. (c): As a comparison, we show characteristic images from an experiment.

4.5 Segregation of monolayers

Cell sorting is one of the fundamental concepts identified that help us to understand processes taking place at various stages of development in a number of organisms. During cell sorting, cells of the same type segregate into disjunct clusters. To explain cell sorting, Steinberg proposed the differential adhesion hypothesis (DAH), suggesting that the process is driven by adhesion differences of the different types of cells involved. Subsequent experiments demonstrated that a surface tension-like quantity can be assigned to cohesive cell clusters and this quantity will predict the spatial arrangement of cell sorting experiments in vitro. The molecular origin of the macroscopic surface tension can be traced back to the surface density of adhesion molecules, primarily cadherins, and a spatially inhomogeneous force generation within the cortical cytoskeleton. The clarity of the DAH made it well suited for theoretical studies in which cell configurations are determined by minimization of the surface energy in a manner similar to a phase separation processes. This insight led to the widespread use of the Cellular Potts Model (CPM) to describe dynamics of multicellular systems, or a variety of multiparticle models which represent intercellular adhesion by a combination of short range repulsive and a somewhat longer range attractive forces.

While the DAH and the corresponding quantitative models for phase separation are useful tools

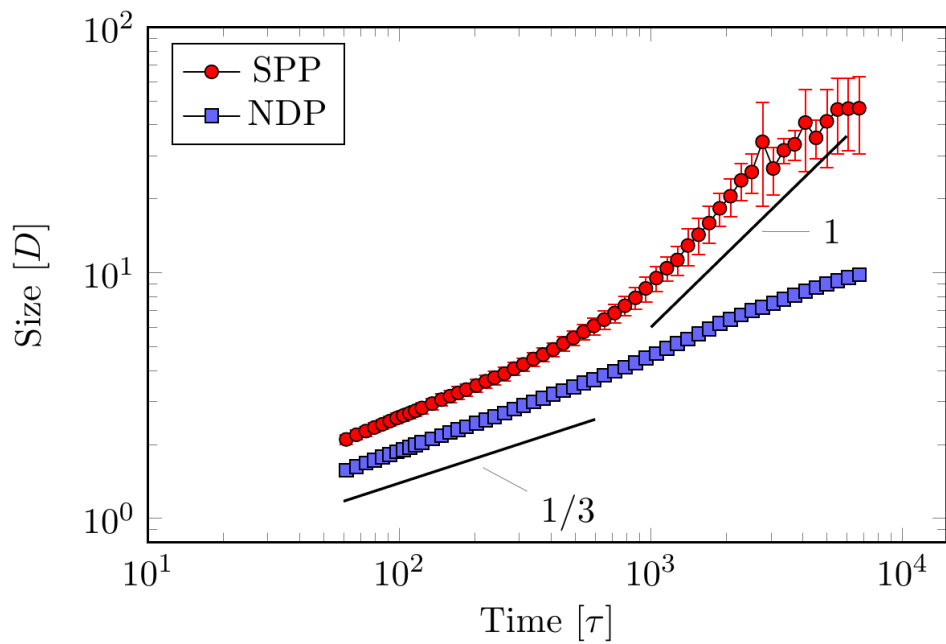


Figure 6: An SPP system can segregate much faster than a similar system containing noise-driven particles (NDP). In NDP simulations the characteristic linear size of the segregated domains grows according to the Cahn-Hilliard behavior. In contrast, the SPP system exhibits a regime where cluster size is proportional to time.

to qualitatively explain cell sorting processes, however, in certain important dynamical aspects our understanding is lacking. Quantitative measures for cell segregation include the characteristic cluster size, D , which is expected to grow in time, t , as

$$D \sim t^{1/3} \quad (1)$$

in the Cahn-Hilliard equation, the usual model for phase separation of binary mixtures. The exponent $n = 1/3$ was recently confirmed for the CPM using large scale simulations. Experiments, however, indicate a much faster segregation dynamics:

$$D \sim t \quad (2)$$

for cell sorting processes both in 3D and 2D. The latter result is of practical importance because the similarities of the experimental setup and the explicit and implicit assumptions of 2D multicellular simulations.

To explain the faster segregation in cellular systems, we utilized a self-propelled particle model without explicit alignment interaction [14]. The main control parameter of the model is the steering quality: for precise adaptation (low noise) the system develops a long-range ordered state where the correlation length of the velocities is comparable with the system size. If the simulations are carried out with two particle types, the interparticle forces can be selected in a way that mirrors cell sorting experimental setups. In particular, we assume that the short range repulsion exists between particles of arbitrary types, the attractive force is limited to particles of the same type. Furthermore, the particle size is represented by the interaction range that separates the attractive and repulsive regimes, this distance was also randomly assigned to each particles from a distribution specific for each cell type. Simulations started with a random binary mixture readily segregate irrespective of the coverage ratio (Fig. 5). Clusters of segregated particles are highly motile and the time development of the segregation process is comparable with that of experiments (Fig.6).

5 Results related to quantitative analysis of multicellular systems, the broader goal of the grant application

5.1 Statistical study on the motility and proliferation of several tumor cell lines

The mortality of patients with solid tumors is mostly due to metastasis that relies on the interplay between migration and proliferation. The go or grow hypothesis postulated that migration and proliferation spatiotemporally excludes each other. In [15] we evaluated this hypothesis on 35 cell lines (12 mesothelioma, 13 melanoma and 10 lung cancer) on both the individual cell and population levels. Following three-day-long videomicroscopy, migration, proliferation and cytokinesis-length were quantified. We reported a significantly higher migration in mesothelioma cells compared to melanoma and lung cancer while tumor types did not differ in mean proliferation or duration of cytokinesis. Strikingly, we found in melanoma and lung cancer a significant positive correlation between mean proliferation and migration. Thus, we demonstrated that the cancer cells studied do not defer proliferation for migration. This data is in line with the observation of pathologists that highly proliferative tumors are often highly invasive as well.

5.2 Fluctuations in the cell differentiation molecular circuit

The maintenance of stem cell pluripotency is controlled by a core cluster of transcription factors, NANOG, SOX2 and OCT4 – genes that jointly regulate each other’s expression. The expression of some of these genes, especially of *Nanog*, is heterogeneous in a population of undifferentiated stem cells. Transient changes in expression levels, as well as heterogeneity of the population is not restricted to this core regulator, but involve a large number of other genes that include growth factors, transcription factors or signal transduction proteins. As the molecular mechanisms behind NANOG expression heterogeneity is not yet understood, in [16] we explore by computational modeling the core transcriptional regulatory circuit and its input from autocrine FGF signaling through the MAP kinase cascade. We argue, that instead of negative feedbacks within the core OCT4/NANOG transcriptional regulatory axis, autocrine signaling loops are likely to generate the observed fluctuations in the expression level of *Nanog* locus.

First we considered various scenarios for the core NANOG circuit and compared their steady state behavior. The transcription and translation rates are chosen in such a way that the steady state transcription factor (protein) concentrations are in the nanomolar range when the promoter is fully active. The nanomolar concentration range is also characteristic for promoter binding affinities, which translate into binding energies around 12 kCal/mol. The transcription factors are assumed to work through stabilizing RNAP II binding – with protein-protein binding energies around 4 kCal/mol range. This binding energy is increased for cooperative, multimolecular complexes. Steady state system behavior was characterized by numerically obtaining intersections of nullcline planes – steady state concentrations obtained when one of the specimen was kept at a fixed value. This analysis of model variants for the core NANOG circuit suggest that it is likely to behave as a bistable system hence the experimentally seen heterogeneity, together with the stability of OCT4 expression levels, is an unlikely consequence of the traditionally considered core NANOG-OCT4-SOX2 dynamics.

To demonstrate that autocrine signaling loops can induce fluctuating *Nanog* expression levels, we consider a feedback through FGFs and ERK. As a particular example, we investigate a scenario in which the stability of the RNAP II complex containing the OCT4/SOX2 dimer depends on ERK activation. Based on known regulatory binding sites, and our rtPCR expression data, we consider the autocrine feedback loop shown in Fig. 7. Using the available transcription factor-DNA binding ChIP data set, we selected two transcriptional regulators for each gene.

The roles KLF4 and ESSRB play in stem cell maintenance is in the focus of recent scientific interest. We demonstrated, that a subset of known interactions is capable to function as an amplifier, greatly expanding the variability of these factors. By keeping NANOG concentrations steady (as input), the autocatalytic expression levels of KLF4 can be well approximated by a Hill function of exponent 2. The steady state expression level of ESSRB is even more non-linear function of [NANOG]: simulated data reveal an even more abrupt switch than a Hill function with $n = 6$.

For strong enough autocrine feedbacks the system is characterized by a fold in the phase space (pitchfork bifurcation), hence small changes in the parameter values can have disproportionately large effects on the steady state concentration values (Fig. 8). Furthermore, due to the hysteresis distinct sub-states can co-exist, and their selection may depend on the history of the system. All these sub-states are, however, within the “On” state of the NANOG core circuit. Thus, we propose that the observed heterogeneity is resulted by slow alterations in model parameters – specific for individual cells – like the feedback strength or the efficiency of autocrine ligand capture.

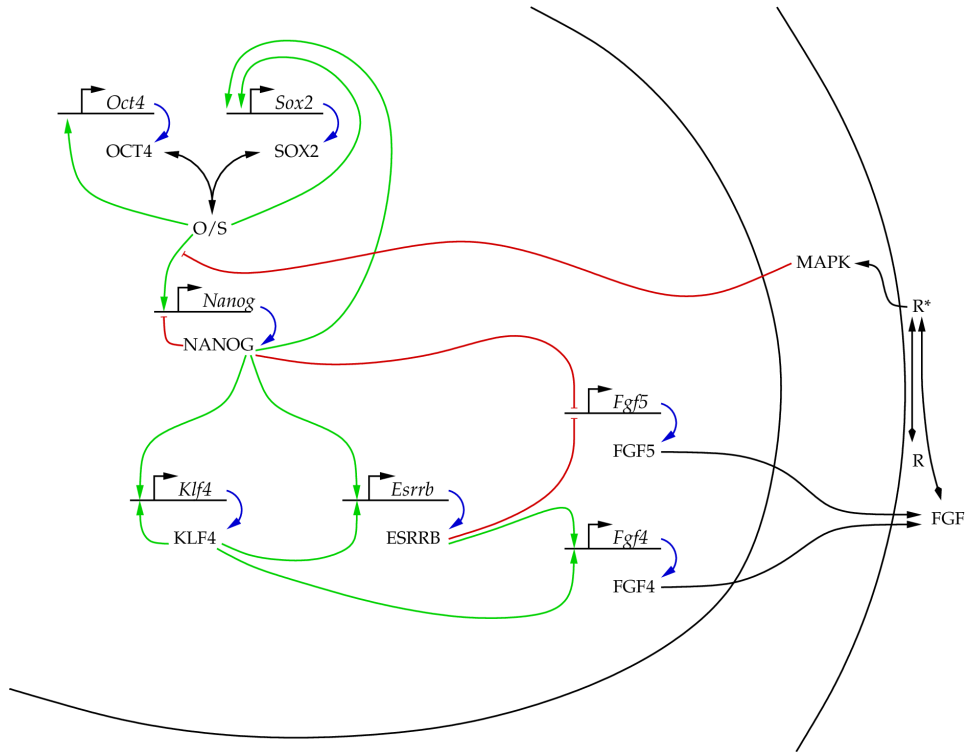


Figure 7: The signaling and transcriptional network considered to regulate mouse ES cell maintenance. Green, red and blue arrows represent transcriptional activation, repression and translation, respectively. Black arrows represent complex formation, and various multi-step processes: (i) FGF secretion resulting in an effective autocrine ligand concentration and (ii) activation of the MAPK.

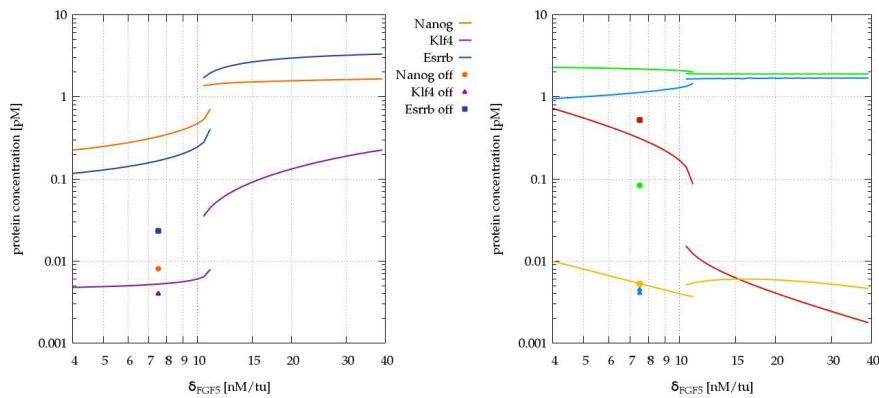


Figure 8: Steady state protein concentrations for strong autocrine feedback as a function of a parameter sensitive to autocrine ligand capture. The abrupt change and the hysteresis indicates the existence of distinct sub-states within the “ON” state of the core NANOG circuit.

References

- [1] A. Szabó, R. Unnep, E. Méhes, W. O. Twal, W. S. Argraves, Y. Cao, and A. Czirók. Collective cell motion in endothelial monolayers. *Phys Biol*, 7(4):046007, 2010.
- [2] A. Czirók, K. Varga, E. Méhes, and A. Szabó. Collective cell streams in epithelial monolayers depend on cell adhesion. *New Journal of Physics*, 15:075006, 2013.
- [3] Katalin Varga, Edina Kosa, and Andras Czirok. Endothelial cell sheet motion is controlled by the persistence of cell polarity and the in-plane shear between cells. *in preparation*, 2013 2013.
- [4] A. Szabó, K. Varga, T. Garay, B. Hegedus, and A. Czirók. Invasion from a cell aggregate—the roles of active cell motion and mechanical equilibrium. *Phys Biol*, 9(1):016010, Feb 2012.
- [5] P.A. Rupp, E. Kosa, and A. Czirok. Fibronectin dynamics during vasulogenesis. *in preparation*, 2013.
- [6] Andras Czirok, Brenda J Rongish, and Charles D Little. Vascular network formation in expanding versus static tissues: Embryos and tumors. *Genes Cancer*, 2(12):1072–1080, Dec 2011.
- [7] A. Szabó, P. A. Rupp, B. J. Rongish, C. D. Little, and A. Czirók. Extracellular matrix fluctuations during early embryogenesis. *Phys Biol*, 8(4):045006, Aug 2011.
- [8] Anastasiia Aleksandrova, Andras Czirok, A. Andras Szabo, Michael B Filla, M. Julius Hosain, Paul F Whelan, Rusty Lansford, and Brenda J Rongish. Convective tissue movements play a major role in avian endocardial morphogenesis. *Dev Biol*, 363(2):348–361, Mar 2012.
- [9] A. Aleksndrova, A. Czirok, E. Kosa, O. Galkin, T. Chevront, and B. Rongish. The endoderm and myocardium join forces to drive early heart assembly: computational modeling confirms distinct roles for both tissues in mediating heart field movements. *submitted*, 2013.
- [10] A. Szabo and A. Czirok. The role of cell-cell adhesion in the formation of multicellular sprouts. *Math Model Nat Phenom*, 5(1):106, Jan 2010.
- [11] Andras Czirok and Charles D Little. Pattern formation during vasculogenesis. *Birth Defects Res C Embryo Today*, 96(2):153–162, Jun 2012.
- [12] Andras Czirok. Endothelial cell motility, coordination and pattern formation during vasculogenesis. *Wiley Interdiscip Rev Syst Biol Med*, 5(5):587–602, 2013.
- [13] Balint Szabo, Renata Unnep, Karoly Marko, Zsuzsanna Kornyei, Elod Mehes, and Andras Czirok. Inhibition of myosin ii triggers morphological transition and increased nuclear motility. *Cytoskeleton (Hoboken)*, 68(6):325–339, Jun 2011.
- [14] A. Mones, E. Czirok and T. Vicsek. Role of active movement in cell segregation. (*in preparation*), 2013.

- [15] Tamas Garay, Eva Juhasz, Eszter Molnar, Maria Eisenbauer, Andras Czirok, Barbara Dekan, Viktoria Laszlo, Mir Alireza Hoda, Balazs Dome, Jozsef Timar, Walter Klepetko, Walter Berger, and Balazs Hegedus. Cell migration or cytokinesis and proliferation? - revisiting the "go or grow" hypothesis in cancer cells in vitro. *Exp Cell Res*, Aug 2013.
- [16] D. Lakatos, J. Vivian, and A. Czirok. Autocrine fgf signaling yields expression heterogeneity of pluripotency gene nanog. *in preparation*, 2013.